Technical Report ARWEC-TR-98008

MECHANICAL FAILURE MODES OF COMPOSITE PLASTIC BONDED EXPLOSIVES

Donald A. Wiegand

November 1998

US ARMY
TANK AUTOMOTIVE AND
ARMAMENTS COMMAND
ARMAMENT RDE CENTER

U.S. ARMY ARMAMENT RESEARCH, DEVELOPMENT AND ENGINEERING CENTER

Warheads, Energetics & Combat-support Armament Center

Picatinny Arsenal, New Jersey

The views, opinions, and/or findings contained in this report are those of the author(s) and should not be construed as an official Department of the Army position, policy, or decision, unless so designated by other documentation.

The citation in this report of the names of commercial firms or commercially available products or services does not constitute official endorsement by or approval of the U.S. Government.

Destroy this report when no longer needed by any method that will prevent disclosure of its contents or reconstruction of the document. Do not return to the originator.

REPORT DOCUMENTATION PAGE

Form Approved
OMB No. 0704-0188

1. AGENCY USE ONLY (Leave Blank)	2. REPORT DATE	3. REPORT TYPE AND DATES COVERED
	November 1998	

4. TITLE AND SUBTITLE
MECHANICAL FAILURE MODES OF COMPOSITE PLASTIC BONDED EXPLOSIVES

5. FUNDING NUMBERS

6. AUTHOR(S)
Donald A. Wiegand

7. PERFORMING ORGANIZATION NAME(S) AND ADDRESS(ES)

ARDEC, WECAC
Energetics and Warheads Division (AMSTA-AR-WEE)
Picatinny Arsenal, NJ 07806-5000

8. PERFORMING ORGANIZATION REPORT NUMBER

9. SPONSORING/MONITORING AGENCY NAME(S) AND ADDRESS(ES)

ARDEC, WECAC
Information Research Center (AMSTA-AR-WEL-T)
Picatinny Arsenal, NJ 07806-5000

10. SPONSORING/MONITORING AGENCY REPORT NUMBER

Technical Report
ARWEC-TR-98008

11. SUPPLEMENTARY NOTES

12a. DISTRIBUTION/AVAILABILITY STATEMENT

Approved for public release; distribution is unlimited.

12b. DISTRIBUTION CODE

13. ABSTRACT

The initial part of the uniaxial stress versus strain response in compression can be described in terms of an undamaged modulus, E_o, a peak stress, σ_m (a failure stress), and a strain at the peak stress, ε_m (a failure strain). σ_m increases in proportion to E_o and ε_m is approximately constant with changes in temperature and strain rate for all of the composites considered. In addition, σ_m increases in proportion to $E_o^{1/2}$ and ε_m is proportional to $1/E_o^{1/2}$ for larger values of E_o for some of the composites. Brittle fracture is often, but not always, observed for the larger values of E_o. These results suggest two separate failure modes, and possible mechanisms for each mode are discussed.

14. SUBJECT TERMS
Plastic bonded explosives, Mechanical failure, Failure strength, Young's modulus, Failure strain, Damage function, Crack growth, Strain energy, Strain rate, Temperature, Strain softening, and Composite

15. NUMBER OF PAGES
28

16. PRICE CODE

17. SECURITY CLASSIFICATION OF REPORT	18. SECURITY CLASSIFICATION OF THIS PAGE	19. SECURITY CLASSIFICATION OF ABSTRACT	20. LIMITATION OF ABSTRACT
UNCLASSIFIED	UNCLASSIFIED	UNCLASSIFIED	SAR

ACKNOWLEDGMENTS

This work was supported in part by Sandia National Laboratories. C. Hu assisted with some of the data collection work. Comp A3 type II data was provided by M. Mezger.

CONTENTS

FIGURES

TABLES

INTRODUCTION

This work was initiated to survey the mechanical properties of a group of particulate polymer composite explosives (refs. 1 through 4). The polymer composites are made up of polymer binders (with plastizer in most cases) and 80% to 95% organic polycrystalline nonpolymer particulate explosives (table 1). The general approach of the work presented was to determine the stress-strain (stress versus strain) properties of these composites as a function of temperature and strain rate. The condition of the samples after deformation was also noted; i.e., whether there was evidence of plastic deformation, cracking, and/or fracture. All of this information was then used in developing insight into the nature of the failure processes.

EXPERIMENTAL

Stress-strain data in compression were obtained using an MTS servo-hydraulic system operated at constant strain rates of 0.001 to 30/s (ref. 5). Samples were in the form of right circular cylinders ¼ in. to 1 in. in length and ¼ in. to ¾ in. in diameter and the end faces of the samples were coated with a lubricant, e.g. graphite, to minimize frictional effects between the sample and the loading platens. Samples were conditioned at temperatures between -60° and 75°C for at least 2 hrs before measurements and were then compressed along the cylinder axis to obtain engineering stress and strain. One to five samples were measured at each temperature and strain rate. However, the curves of figures 1 and 6 and the points of figures 2 through 5 each represent one sample.

Samples of the polymer composite explosives were prepared either by pressing to size or by pressing into large billets and machining to size (refs. 1, 2, and 6). Precautions were taken to insure that the cylinder end faces were flat and parallel. The densities of all samples were measured and results are presented only for samples having densities in a narrow range close to the maximum theoretical (zero porosity) density.

In table 1, the composition of the explosive composites considered are given. Glass transition temperatures, T_g, are given where known.

RESULTS

For uniaxial compression of the materials of the table, the stress initially increases linearly with increasing strain then curves over and passes through a maximum stress with further increases in strain as shown in figure 1. The stress either decreases continuously for additional increases in strain beyond the maximum in the strain-softening region (fig. 6), or in some cases, at the lowest temperatures the stress decreases abruptly to near zero for strains at or just beyond the maximum as indicated schematically in figure 1. In some cases, there is non-linearity at the very beginning of the stress-strain curve due to sample end conditions (not shown in figure 1). Failure is considered here to initiate at the point given by σ_f and ε_f in figure 1, where the stress-strain curve deviates from linearity. Stresses up to about this point do not cause permanent changes, while stresses beyond this point do cause permanent changes (ref. 7). However, this point is often difficult to locate precisely because of noise and curvature. Therefore, the maximum stress, the compressive strength, is used here as a measure of the failure stress, and the strain at the maximum stress is

used as a measure of the failure strain. For the data of figure 1, this is approximately equivalent to using a 0.4% strain offset as a definition of failure. Three quantities taken from the initial part of the stress-strain curves are of interest:

- The initial slope, which is taken as a measure of the undamaged modulus, E_o
- The maximum compressive stress (the compressive strength), σ_m, taken as a measure of the failure stress
- The strain at the maximum stress, ε_m, taken as a measure of the failure strain (fig. 1).

After strains much greater than ε_m, the samples appear to be plastically deformed and/or macroscopically cracked, and in some cases fractured. Fractured, as used here, means broken into separate pieces. In those cases at lower temperatures where the stress has dropped abruptly to near zero at or near the maximum (fig. 1), the samples are always fractured, and in some cases (e.g., PAX 2 and PAX 2A) they are fragmented into many pieces.

In figures 2 and 3, the log of the compressive strength, σ_m, is given versus the log of the modulus, E_o, for PAX 2A and for LX-14, respectively. Data is given for temperatures between -45°C to 65°C and for strain rates between 0.001/s and 1.0/s. For the smaller values of the modulus, the compressive strength increases linearly with the modulus while for the larger values, the strength increases as the square root of the modulus. Linear plots (not shown) of σ_m versus E_o (refs. 2 and 3) and σ_m versus $E_o^{1/2}$ for the appropriate regions of figures 2 and 3, give straight lines that pass through the origin. These results suggest two separate failure modes or branches: a failure mode with the failure strength, σ_m, proportional to E_o for smaller values of E_o, designated here as the linear failure mode and a failure mode with σ_m proportional to $E_o^{1/2}$ for larger values of E_o, designated here as the square-root failure mode. This conclusion is supported by the observations that the compressive strength is exponen-tially dependent on 1/temperature (1/K) with two activation energies: one for the region of the linear failure mode and another for the region of the square-root failure mode (ref. 8). The latter activation energy is one half of the former. The modulus is also exponentially dependent on 1/temperature (1/K), but with the same activation energy throughout both regions and with a value equal in magni-tude to the value for the strength in the linear mode (ref. 8). The temperature and strain rate depen-dencies of the modulus are thought to be primarily associated with the viscoelastic properties of the binder.

For a given value of E_o, it appears that the failure mode (linear or square root) is determined by the mode that requires the lower value of failure stress, i.e., the compressive strength. Therefore, for values of log E_o less than about 2.65 for PAX 2A (fig. 2), the linear mode requires the lower stress while for values of log E_o greater than 2.65 the square root mode requires the lower stress. Similar considerations apply to the data for LX-14 in figure 3. The linear mode was observed for all of the composites of the table, but the square root mode was observed only for PAX 2, PAX 2A, LX-14, and to a limited extent for 9404 and Comp A3 Type II. All of the available data for 9501 lies in the linear range, while the available data for 9502 for the larger modulus range does not conform to either a linear or a square route relationship. N9 is anomalous in that the stress-strain curve before the maximum (fig. 1), indicates two approximately linear regions and so two slopes. The slope at the larger strain is greater than the initial slope. The peak stress is proportional to the initial slope and so indicates the linear failure mode. Several other composites and TNT also exhibit the linear failure mode (ref. 3). The square root branch may not have been observed to date in some of the

composites because the stress and the moduli required may be greater than those encountered experimentally. Lower temperatures and/or higher strain rates may then be necessary to observe this branch in these composites.

From the stress-strain curve of figure 1, a geometric relationship between the three quantities σ_m, E_o, and ε_m can be obtained as

$$\sigma_m = E_o \varepsilon_m /(1 + a) \quad (1)$$

where σ_m (1 + a) is the stress at which a straight line through the initial portion of the stress-strain curve, the slope of which defines E_o, intersects a constant strain line at ε_m (ref. 2). The parameter **a** is a measure of the shape of the stress-strain curve between the point where it deviates from a straight line and the point of maximum stress. In all cases where a linear relationship between σ_m and E_o is observed, ε_m is found to be approximately constant (refs. 1 through 4) as illustrated in figure 4 for PAX 2A and in figure 5 for LX-14 for the smaller values of E_o (larger values of $1/E_o^{1/2}$). While the parameter **a** does change somewhat with temperature and strain rate, the magnitude of the changes in **a** are such that equation 1 is satisfied with an approximately constant ε_m for all the materials of the table and in the temperature and strain rate range such that σ_m is proportional to E_o. For PAX 2A, the parameter **a** has a maximum as a function of temperature in the low temperature range and the temperature of the maximum increases with strain rate. This may contribute to the apparent scatter of the data of figure 4 in the low temperature (large E_o) range. The data for LX-14 and the other materials are not sufficiently extensive to determine if similar maxima in the parameter **a** occur.

Although ε_m is approximately constant (compared to the changes in σ_m and E_o) with changes in temperature and strain rate in the ranges for the linear failure mode, there is a tendency for this strain for some of the materials to increase slightly with decreasing temperature and increasing strain rate.

Substituting $\sigma_m = K E_o^{1/2}$ into equation 1 for the square route branch and rearranging gives

$$\varepsilon_m = K (1 + a)/E_o^{1/2} \quad (2)$$

This equation is satisfied for the appropriate values of E and for those composites which exhibit the square route branch. This is also illustrated for PAX 2A in figure 4 and for LX-14 in figure 5 for the larger values of E (smaller values of $1/E^{1/2}$).

DISCUSSION

Studies of the uniaxial stress-strain behavior following prior uniaxial deformation (and so damage) indicate that for maximum prior strains in the initial linear region of the stress-strain curve (fig. 1), a change in the modulus is not detected. However, for maximum prior strains exceeding this linear range, the modulus decreases continuously with increasing prior strain and so amount of damage (ref. 7 and 9). These results indicate that the stress-strain response of figure 1 and well into the softening region (fig. 6) can be attributed to a damage modulus that decreases continuously with increasing strain beyond the linear range (refs. 7 and 9). Therefore, the uniaxial stress-strain response can be expressed as

$$\sigma = E\,\varepsilon = (E_o - \Delta E)\,\varepsilon = \varepsilon/Y = \varepsilon/(Y_o + \Delta Y) \tag{3}$$

where E is Young's modulus, Y is the compliance, E_o and Y_o are the values before damage due to loading, and ΔE and ΔY are the changes due to damage introduced by loading. To first order $\Delta E/E_o = \Delta Y/Y_o$. ΔY is assumed to be a single-valued monotonically increasing function of ε. Y_o and ΔY may be functions of temperature, strain rate, initial crack and dislocation parameters, density, etc. However, all damages (e.g., changes in crack and dislocation parameters) is assumed to be expressed through the dependence of ε on these changes. Dienes (ref. 10) and Dienes and Riley (ref. 11) used equation 3 with several models for the dependence of ΔY on crack parameters in fitting the author's data for 9501.

By differentiating σ of equation 3 with respect to ε, and setting the resulting differential equal to zero, the condition for a maximum in the curve of σ versus ε is found to be

$$\varepsilon_m = (Y_o + \Delta Y_m)/\,\Delta Y_m' \tag{4}$$

where the subscript m denotes the values at the maximum and the ' symbol indicates differentiation with respect to ε, e.g., $\Delta Y_m' = [d(\Delta Y)/d\varepsilon]_m$. By substitution of equation 4 into 3, the stress at the maximum is

$$\sigma_m = 1/\Delta Y_m' \tag{5}$$

From equation 4, $\Delta Y_m'$ must be non-zero and positive. Thus, ΔY_m must be an increasing function of ε as assumed.

To satisfy the linear branch of the σ_m versus E_o curve, it is then necessary for $\Delta Y_m'$ to be expressed as

$$\Delta Y_m' = Y_o\, f(\varepsilon_m)' = f(\varepsilon_m)'/E_o \tag{6}$$

with $f(\varepsilon_m)'$ independent of or insensitive to temperature and strain rate. It is assumed here that the initial linear slope of the stress-strain curve is given by E_o. Substitution of equation 6 into 4 yields

$$\varepsilon_m = (Y_o + \Delta Y_m)/Y_o\, f(\varepsilon_m)' \tag{7}$$

If

$$\Delta Y_m = Y_o f(\varepsilon_m) \tag{8}$$

ε_m is independent of or insensitive to temperature and strain rate in agreement with the experiment. Thus, the relationships for σ_m and ε_m are

$$\sigma_m = E_o/f(\varepsilon_m)' \tag{9a}$$

and

$$\varepsilon_m = (1+ f(\varepsilon_m))/f(\varepsilon_m)' \quad (9b)$$

where $f(\varepsilon_m)$ and $f(\varepsilon_m)'$ are independent of or insensitive to temperature and strain rate.

If $f(\varepsilon)$ is valid at all strains and is expressed as a power series in ε, the condition that there is a maximum in the σ versus ε curve is that the highest power of ε is greater than unity. The total compliance from equations 3 and 8 is then given by

$$Y = Y_o(1 + f(\varepsilon)) \quad (10)$$

so that

$$(1 + f(\varepsilon)) \quad (11)$$

is a damage function for the compliance.

In summary, by expressing the total compliance as the sum of the undamaged compliance and the change in compliance due to damage, and by comparing the resulting equations for σ_m and ε_m with the experimental results, it is concluded that the change in compliance is proportional to the undamaged compliance (eq. 8) and further that the damage function is primarily a function of the total strain and is independent of or insensitive to temperature and strain rate. Other conclusions may be possible.

The linear branch of the σ_m versus E_o curve and the attendant constant ε_m have been discussed elsewhere in terms of either a constant strain as the criterion for failure or in terms of an unspecified mechanism requiring σ_m to be proportional to E_o (refs. 2 and 3). From equation 1, a constant ε_m results in σ_m being proportional to E_o and conversely if σ_m is proportional to E_o, ε_m must be constant, all if the parameter **a** is constant. This damage approach provides a rationale for a constant strain criteria for failure with changes in temperature and strain rate (eq. 9b) based on a damage function that is independent of or insensitive to these two parameters in the initial stages of damage (eq. 11). In addition, the linear relationship between σ_m and E_o is obtained (eq. 9a). Therefore, this damage approach satisfies the experimental criteria. This damage mechanism also, of course, provides the rationale for why σ_m has the same temperature and strain rate dependencies and so activation energy as E_o in the linear failure mode range (ref. 8). As noted, the temperature and strain rate dependencies of E_o are thought to be due primarily to the viscoelastic properties of the binder.

Results at 25°C and a low strain rate also indicate that if the strain does not exceed a strain of about ε_f (fig. 1), a change in the modulus within the precision of the measurements is not detected. However, if ε_f is exceeded, the modulus is decreased as noted (ref. 7 and 9). Therefore, the damage function (eq. 11) may, at least for practical purposes, have a damage threshold ε_f. The threshold stress, σ_f, then varies linearly with the modulus as temperature and strain rate vary. Further work in this area is desirable.

While additional work is necessary to establish the nature of the damage, the conclusions that the change in compliance is proportional to the undamaged compliance and that the damage function is independent of or insensitive to temperature and strain rate places significant restrictions on the possibilities. Thermally-activated slow-crack growth is not a possibility because the function $f(\varepsilon)$

(eq. 8) is not a function of temperature and strain rate (refs. 5 and 8). Brittle fracture of particulate particles, perhaps involving particle interactions, may under some circumstances satisfy the necessary conditions. Evidence for decreased particulate particle sizes in several of the composites of the table after damage by uniaxial compression were found by small angle x-ray and neutron scattering (ref. 12). While the author is unaware of mechanical property measurements for any of the composites of the table as a function of particulate particle size, measurements were made of pressed HMX, the particulate for most of the composites of table 1, for two different average particle sizes (ref. 13). Samples containing only coarse HMX gave moduli and compressive strengths higher by about 30% compared to samples containing a bimodal mixture of coarse and fine particles sizes in the ratio 3/1. Both sample groups were pressed to approximately the same density. In contrast, measurements of samples of an inert simulant of 9501 containing sugar in place of HMX, and with the same two particle size distributions as for the HMX discussed previously, did not show differences in the moduli or the compressive strengths (ref. 14). Measurements of the moduli and the particle sizes for the composites of the table as a function of deformation or other variables are desirable to further resolve this matter.

A normalized stress-strain relationship can be obtained from equations 3, 5, and 8 as

$$\sigma/\sigma_m = \varepsilon\, f(\varepsilon_m)'/(1+ f(\varepsilon)) \qquad (12)$$

Therefore, to the extent that the equations used to obtain equation 12 are valid at strains other than ε_m, this normalized stress-strain relationship is independent of or insensitive to temperature and strain rate if $f(\varepsilon)$ and $f(\varepsilon_m)'$ are independent of or insensitive to temperature and strain rate. An examination of the data indicates that the normalized stress-strain curves are relatively insensitive to temperature and strain rate in the initial linear region and in the vicinity of the maximum, but are more sensitive to these variables in the softening region. This is illustrated in figure 6 by normalized stress-strain curves for LX-14 at 65°C for several strain rates. The differences in the softening region indicate a rather strong strain rate effect while the slopes (moduli) in the initial region and the strains at the maxima indicate a minimal strain rate dependence. The strain rate dependence in the softening region decreases with decreasing temperature and is minimal at the lowest temperatures (not shown). Some of the differences in the initial region before the maxima are due to deviations of the sample end surfaces from flatness and parallelism. In general, similar results were obtained for other composites of the table. However, it is important to note that the samples are not damaged uniformly along the sample length in the softening region. After loading into the softening region, the samples are often barreled, i.e., the permanent radial expansion is less at the sample ends than in the mid-section. This effect is due to the frictional constraints on the radial expansion of the sample ends by the compression platens. This occurred even though lubrication was used on the sample ends to minimize this friction. Therefore, the observed stress-strain curves are averages over ranges of damage. The softening region of the stress-strain curves will be treated in more detail elsewhere (ref. 15).

Dienes and Riley (ref. 11) have used equation 3 with Y expressed in the form of equation 10 and $f(\varepsilon) = k\,\varepsilon^3$, as obtained from a very simple crack propagation model, to fit this author's data for 9501 for a range of temperatures and strain rates. Y_o (E_o) and k were varied to give the best fits to the stress-strain curves for strains between zero and 0.04, the latter being well into the softening region of the curves. The fits to the data with k and E_o dependent on temperature and strain rate are surprisingly good considering the simplicity of the model. However, the model predicts a much stronger dependence of k on strain rate than obtained by fitting to the data and the fits to the initial

portions of the stress-strain curves of immediate concern here are in several cases not as good as might be desired. The model predicts ε_m to be dependent on k and so temperature and strain rate. In addition, the model predicts σ_m to be proportional to E_o as observed, but also predicts σ_m to be dependent on k. In particular, this dependence of σ_m on k and so temperature and strain rate, in addition to the dependence of σ_m on temperature and strain rate through E_o, is contrary to observations (figs. 2 and 3). The temperature dependence of k is not discussed by Dienes and Riley (ref. 11). As noted, the normalized curves are insensitive to temperature and strain rate for the initial parts of the curves but are temperature and strain rate dependent in the softening region (fig. 6). A more complex model may be necessary to fit the data in the initial regions and in the softening region. Dienes and Riley also fit some of this author's 9501 data to a more complex crack model with realistic crack parameters, but the fits are not as good as the fits with the simpler model (ref. 11). The goal of this latter fitting was to deduce information on the microstructure, e.g., crack size and number density. These are used in a hot-spot analysis of ignition associated with mechanical deformation. Unfortunately, these authors used a form of the data for all of their curve fitting that was not corrected for measuring system compliance. This correction influences the data primarily at lower temperatures (larger stresses).

Aidun has developed a phenomenological viscoelastic model for 9501 based on maxwell elements (ref. 15). A damage function was deduced to account for the difference between this author's 9501 data at 25°C and the viscoelastic model. Reasonably good fits were obtained over essentially the entire stress-strain curves by using a damage function which is strain rate independent in the initial parts of the curves up to about the maxima (fig. 1), but which is strain rate dependent in the softening region at greater strains. This strain rate dependence of the damage function is consistent with this discussion of the parameter k used by Dienes and Riley (ref. 11). Temperature variations were not considered by Aidun.

In addition, Gozonas has developed a nonlinear viscoelastic model with damage due to slow crack growth which he has fitted to M30 propellant data as a function of temperature and strain rate for strains in the vicinity of and greater than ε_m (refs. 16 and 17). M30 has similar mechanical properties to the materials considered here (ref. 3). The agreement between the model and the data is reasonably good for this range of strains and does include the observed constant failure strain, ε_m (refs 3 and 16). However, the model was not fitted to the initial linear part of the stress-strain curve defining E_o and does not appear to predict this part of the curve very well. Therefore, the model does not predict the observed linear relationship between σ_m and E_o (ref. 3).

The approach used here for the linear mode, based on a damaged compliance, is not readily adaptable to the square root failure branch of the σ_m versus E_o curve. There are, however, other possible reasons for the square root relationship between σ_m and E_o not directly involving damage functions, but instead failure criteria. Consider first the total work per unit volume, W_v, performed in uniaxial compression. W_v can be expressed as

$$W_v = \int \sigma d\varepsilon \tag{13}$$

Equation 13 can be written as

$$W_v = 1/E_o \int \sigma d\sigma = (\sigma_f)^2/2E_o \tag{14}$$

when the integration is over the initial linear portion of the stress-strain curve from zero stress to a failure stress σ_f taken at the point where the curve (fig. 1) deviates from linearity. Then from equation 14

$$\sigma_f = (E_o)^{1/2} (2W_v)^{1/2} \quad (15)$$

is obtained. For an elastic material W_v is equal to the total elastic energy per unit volume, U_v. However, because the materials in question were found to have viscoelastic properties (ref. 9), the elastic energy will be a fraction r of W_v. Therefore, equation 15 can be written as

$$\sigma_f = (E_o)^{1/2} (2U_v/r)^{1/2} \quad (16)$$

With σ_m taken as a measure of σ_f, equation 16 gives the observed relationship between σ_m and E_o if (U_v/r) is constant as temperature and strain rate are varied over the limits of the square root region of the σ_m versus E_o curve (figs. 2 and 3). For elastic materials (r=1), equation 16 gives the relationship between the failure stress and E_o for a total maximum elastic strain energy criterion for failure (ref. 18). A similar relationship is obtained for the elastic energy of distortion criterion and the equivalent maximum octahedral shearing stress (von Mises) criterion for failure (ref. 18). But, because r is not constant for viscoelastic materials, it appears that these failure criteria are not applicable to the materials in question. However, before concluding that these failure theories are not in fact applicable because of variations in r, it is necessary to determine experimentally the magnitude of the changes in r over the range of temperature and strain rate of interest.

Additional measurements are necessary to distinguish between the several failure criteria mentioned here. It should be possible to distinguish between a constant total strain energy criteria and a constant strain energy of distortion criteria by comparing the results of torsion tests with the uniaxial results (ref. 18). The total strain energy criteria is, however, unlikely because failure has not been observed in other materials for hydrostatic compression to total strain energies significantly higher than the value for uniaxial failure (ref. 18).

Consider next the Griffith condition, which in contrast, is related to the decrease of the total strain energy due to crack growth and occurs when this decrease is equal to the increase in the surface energy also due to crack growth. Frictional effects between fracture surfaces are neglected. The Griffith condition may be stated as

$$\sigma_g = [\gamma E_o K/c]^{1/2} \quad (17)$$

where σ_g is the stress required for crack growth, c is the crack length, γ is the surface energy per unit area, and K is a numerical constant (ref. 19). While equation 17 is valid for a particular set of conditions which differ from the experimental conditions used here, the relationship between the stress and the modulus should be generally valid since it is obtained from the relationship for the strain energy. Because of this relationship, the slope of the square root branch (figs. 2 and 3) is then a function of the (maximum) crack length c for this mechanism of failure. This dependence on the maximum crack length could explain the large scatter of the experimental points of figure 2 for this branch because of variations of maximum crack length from sample to sample. Measurements of failure strength as a function of crack length are desirable to determine if the square root branch is indeed due to the Griffith condition for crack growth. A characteristic of this crack growth (without crack arrest) is abrupt fracture as indicated by a sharp decrease of the stress to zero or near zero with increasing strain. Although abrupt fracture (fig. 1) is observed at the lowest temperatures (large E_o) for most of the composites exhibiting the square root branch, it is not observed for all of the

composites having this branch and is not observed for many of the points lying on this branch (figs. 2 and 3). Thus, if the square root branch is due to the Griffith condition for crack growth, it must be concluded that crack arrest is also important in many cases because of this lack of abrupt fracture. Damage must be accumulated by this crack growth and arrest and in some cases apparently leads to eventual abrupt fracture at the lowest temperatures.

It is, therefore, possible to interpret the initial part of the stress-strain response in terms of deformation-induced damage that is detected as increased compliance. The incremental compliance (due to damage) is proportional to the undamaged compliance and the damage function is determined either exclusively or primarily by the total strain and is independent of or insensitive to temperature and strain rate. This interpretation applies to the composites of table 1 and some other materials (ref. 3), all of which give linear relationships between the maximum stress, σ_m, and the modulus, E_o and a constant or almost constant ε_m. In addition, as just considered, some of the composites of table 1 appear to exhibit another mechanism which produces failure at larger E_o (lower temperatures and/or higher strain rates) at significantly lower stresses than the stresses required for this damage process. In these cases, σ_m varies as the square root of E_o. This type of relationship can be associated with the Griffith conditions for crack growth, with a critical total strain energy for failure or with a critical strain energy of distortion for failure. It, therefore, appears that for some of the composites, there is a shift from a strain-dependent damage mechanism to a stress dependent failure process as the temperature is lowered and/or the strain rate is increased. The results also indicate that for any given set of conditions of temperature and strain rate and so modulus E_o, the failure process which is dominant (i.e., with σ_m proportional to either E_o or $E_o^{1/2}$) is the process that requires the lower stress. Additional work is required to further establish the nature of these failure processes.

SUMMARY

The results suggest two failure modes or branches in the temperature and strain rate ranges studied, a lower modulus mode in which the failure strength is proportional to the modulus and the failure strain is (approximately) constant, and a higher-modulus mode in which the failure strength is proportional to the square root of the modulus and the failure strain decreases as the modulus increases. The lower modulus mode, which was observed for all of the composites studied, occurs at higher temperatures and lower strain rates while the higher modulus mode, which was observed only for some of these composites, occurs at lower temperatures and higher strain rates. The results suggest that the lower modulus mode can be attributed to a damage compliance with the change in compliance proportional to the undamaged compliance and a damage function that is strain dependent and is independent of or insensitive to temperature and strain rate. The results further suggest that the criterion for failure for the higher modulus mode is either a constant strain energy or a critical stress for crack growth. Additional work is indicated.

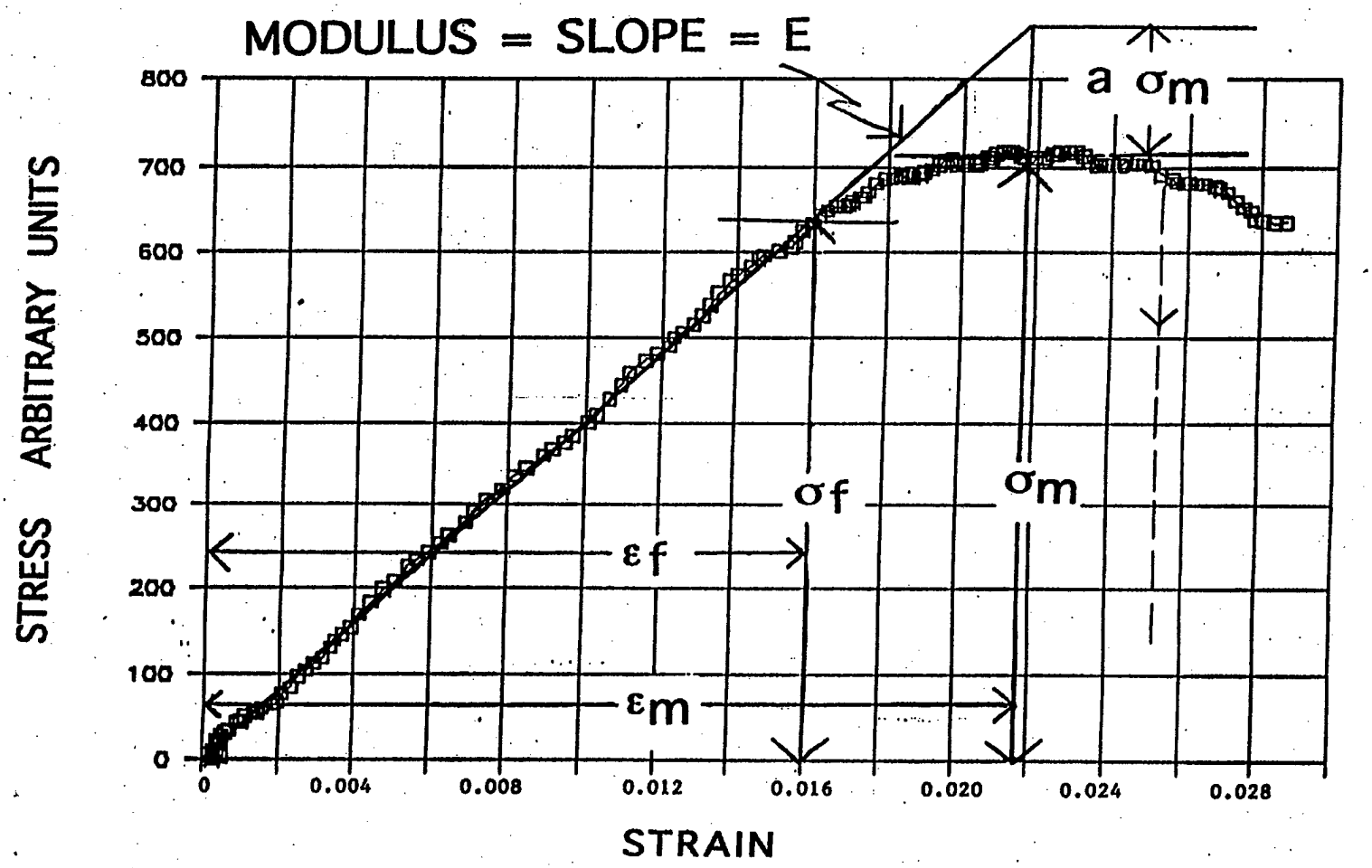

Figure 1
An example of the stress versus strain response for the composites of table 1 for most temperatures and strain rates. The dashed line indicates schematically the decrease of the stress at the lowest temperatures for some of the composites.

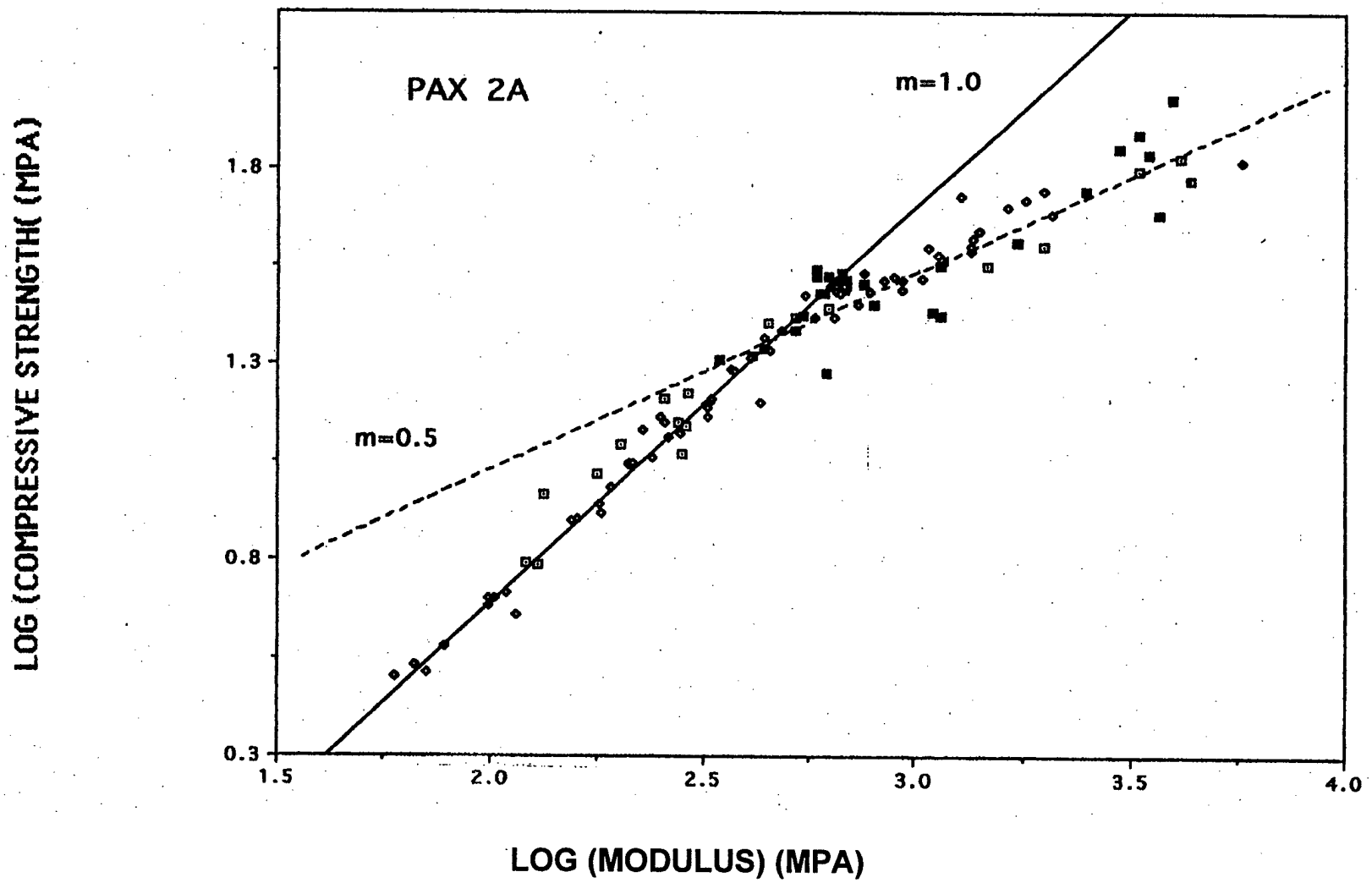

Figure 2
Log of the compressive strength versus log of Young's Modulus for PAX 2A.
The straight lines were drawn in with the indicated slopes.

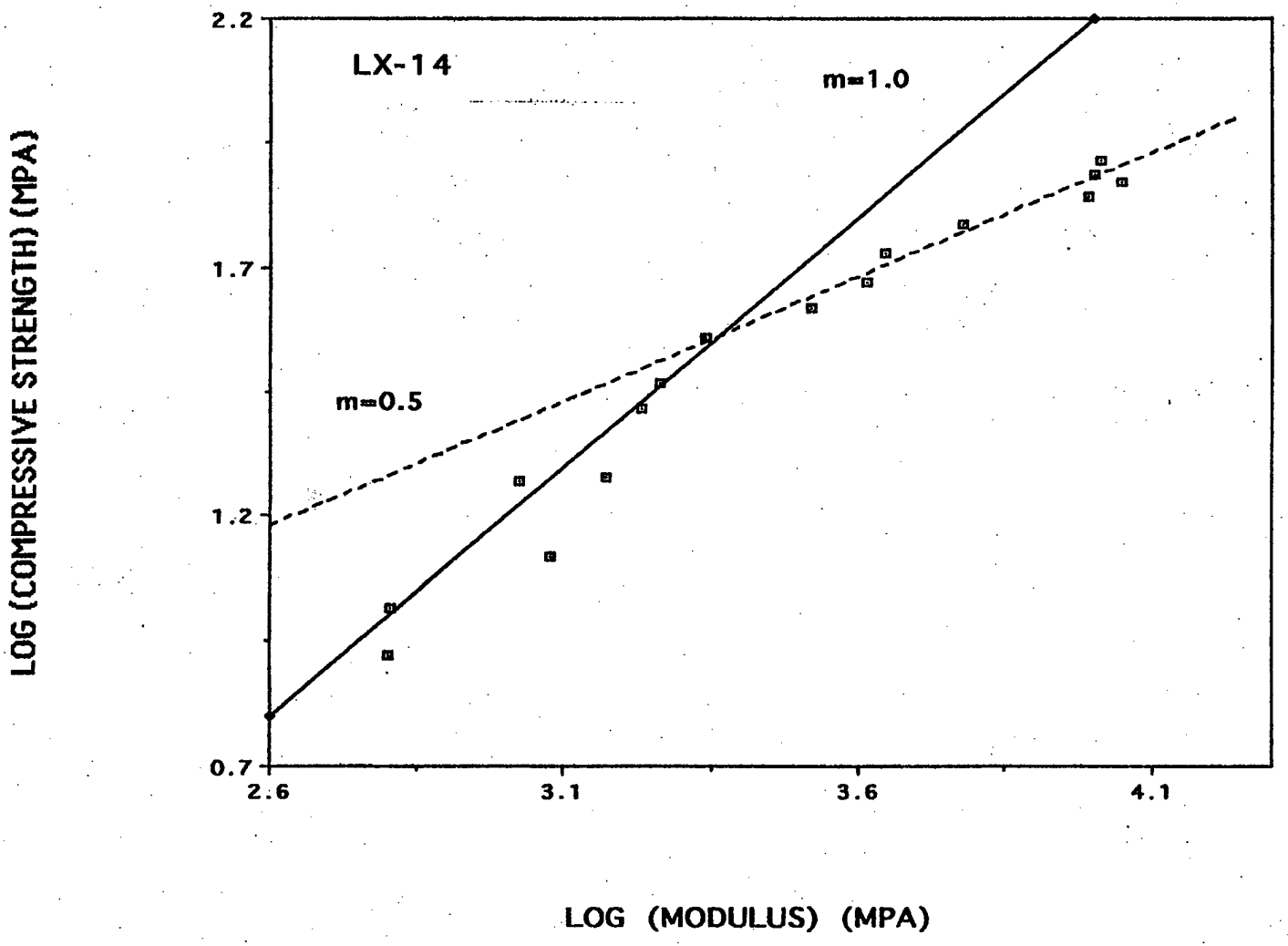

Figure 3
Log of the compressive strength versus log of Young's Modulus for LX-14.
The straight lines were drawn in with the indicated slopes.

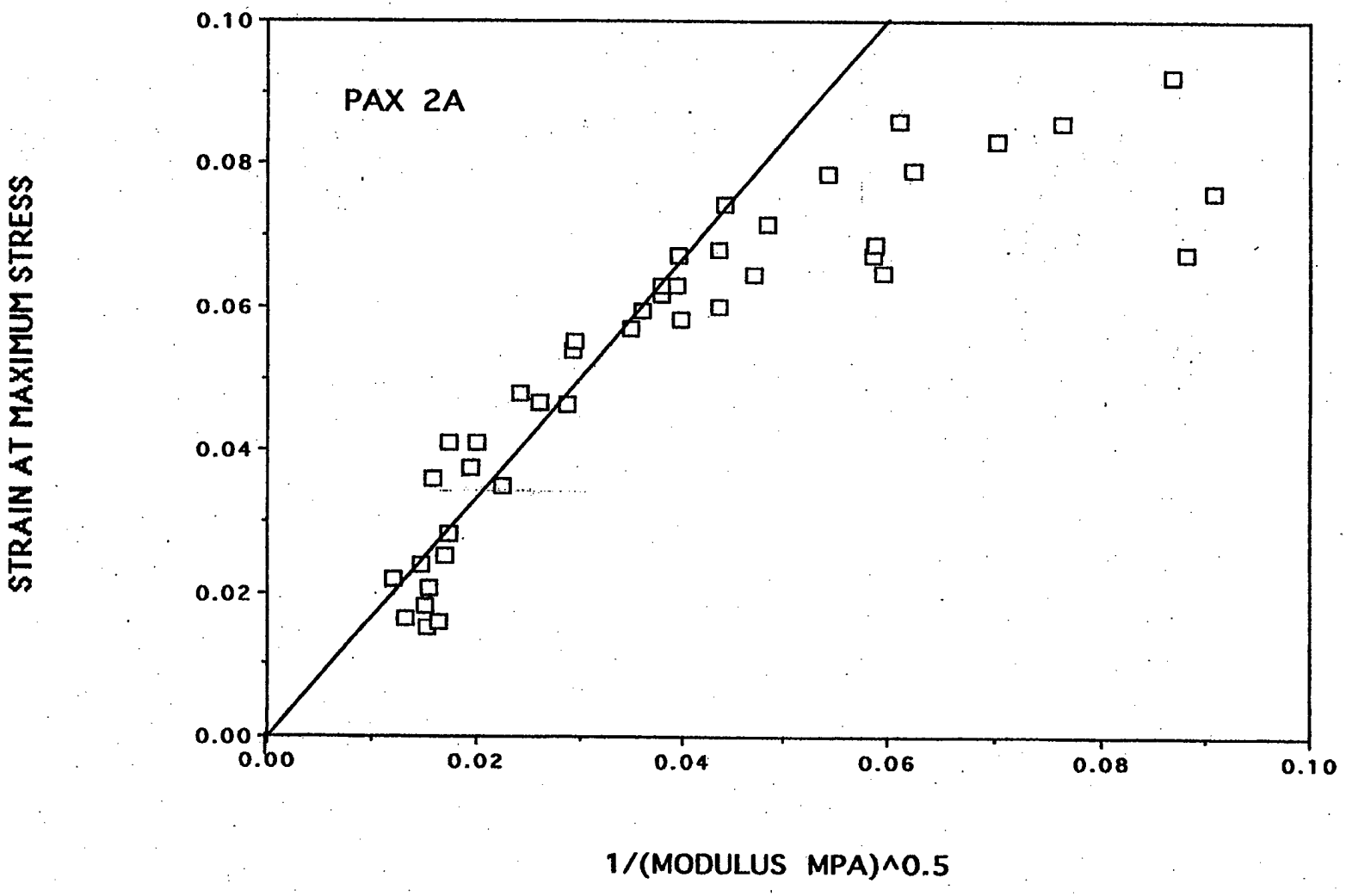

Figure 4
Strain at the maximum stress versus the reciprocal of the square root of the modulus for PAX 2A
The straight line was fitted to the data points for $1/(E_o)^{0.5}$ values from 0 to 0.04 with R^2=0.878.

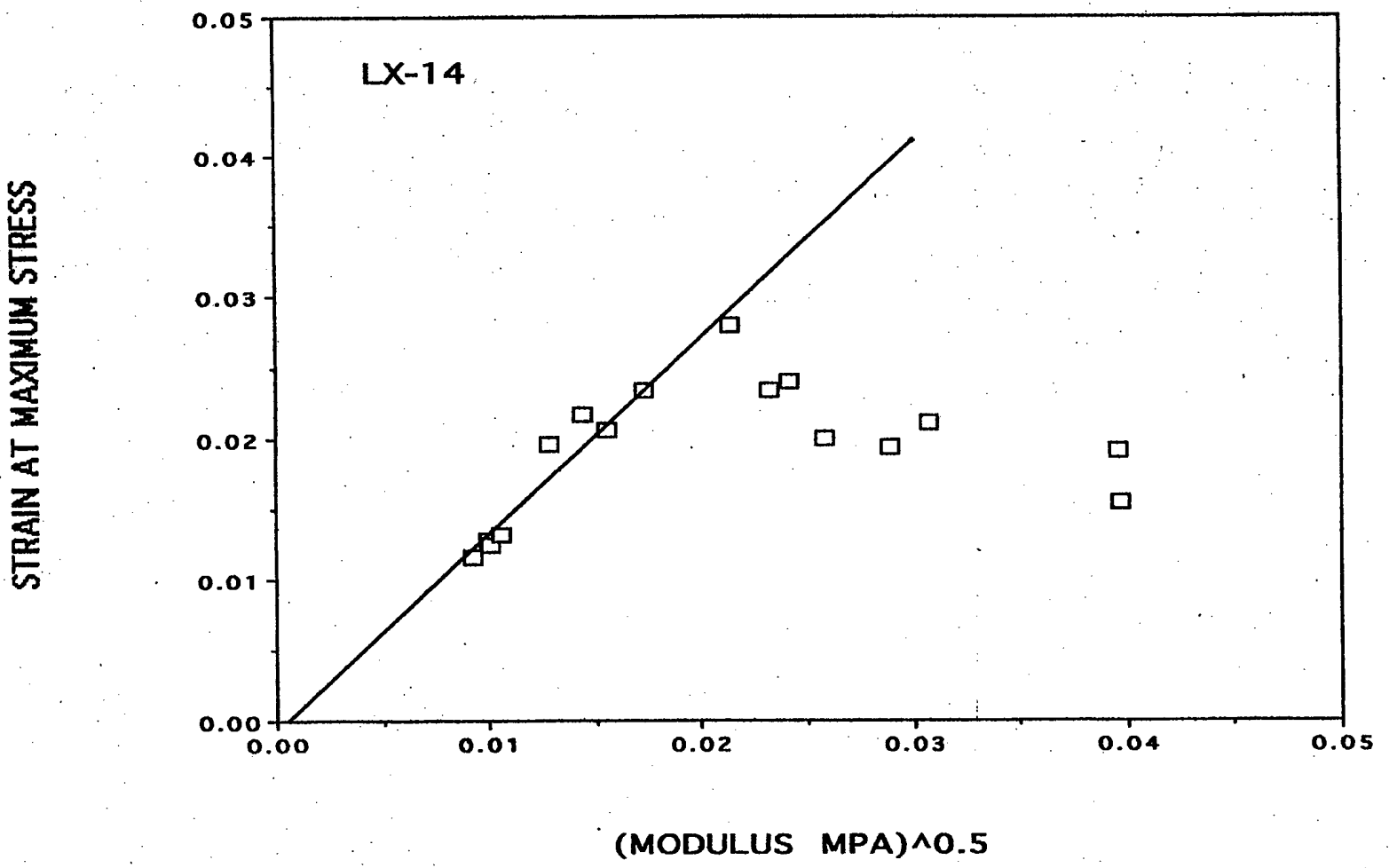

Figure 5
Strain at the maximum stress versus the reciprocal of the square root of the modulus for LX-14.
The straight line was fitted to the data points lying along the line with R^2=0.948.

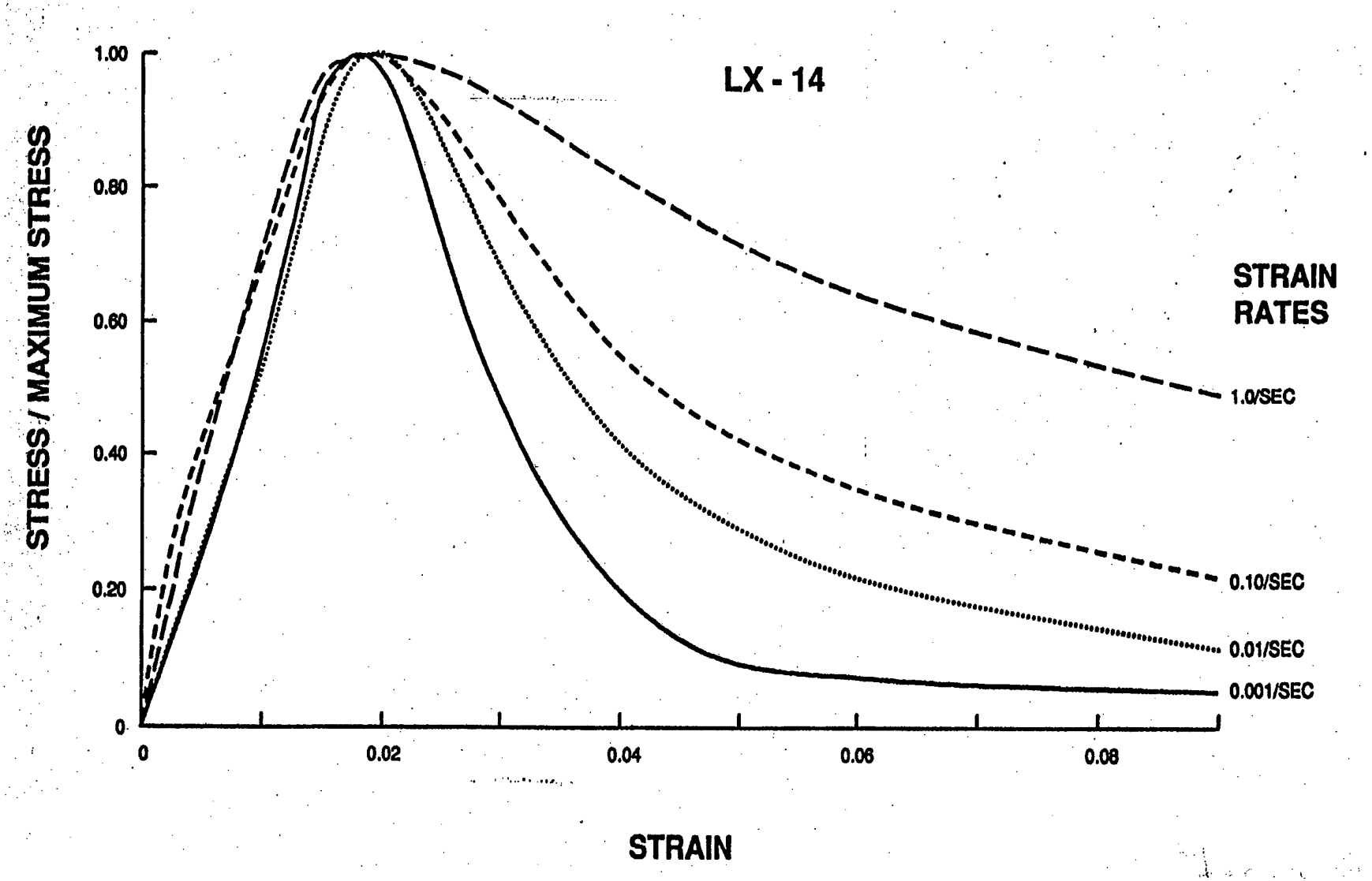

Figure 6
Stress versus strain curves normalized to the maximum stress for LX-14 at 65°C for several strain rates

Table 1
Composition of particulate polymer composites

	Name	Particulate	Binder		Tg (°C)
			Polymer	Plastizer	
I	Pax 2	HMX 80%	CAB 8%	BDNPA/F 12%	-37[a]
II	Pax 2A	HMX 85%	CAB 6%	BDNPA/F 9%	-37[a]
III	9404	HMX 94%	NC* 2%	CEF 3.84%	-34[b]
IV	9501	HMX 95%	ESTANE 2.5%	BDNPA/F 2.5%	-41 (B)[c]
V	9502	TATB 95%	KEL F 800 5%		30 (B)[b]
VI	LX-14	HMX 95.5%	ESTANE 5702-F1 4.5%		-31 (B)[b]
VII	Comp A3	RDX 91%	POLYETHYLENE 9%		
VIII	N9	HMX 92%	HYCAR 4454 2%	DOA 6%	-43[d]

Nomenclature: HMX - Cyclotetramethylene tetranitramine.
TATB - 1,3,5-triamino-2,4,6-trinitrobenzene.
RDX - Cyclotrimethylene trinitramine.
NC - Nitrocellulose. NG - Nitroglycerine.
CAB - Cellulose Acetate Butyrate.
BDNPA/F -Bis(2,2-Dintropropyl)Acetal/Formal.
CEF - Tris(Beta Chloroethyl) Phosphate.
Estane - Polyurethane.
KEL F 800 - Chlorotrifluoroethylene/vinylidine flouride copolymer.
DOA - Dioctyl adipate.
B - Property of the binder.
* Also contains 0.1% Diphenylamine

[a] Personal Communication, J. Harris, Picatinny Arsenal, N.J.
[b] Reference 20.
[c] Reference 21.
[d] Reference 22.

REFERENCES

1. Wiegand, D., Hu, C., Rupel, A., and Pinto, J., "Fracture and Yield of Several Highly Filled Polymers", 9th International Conference on Deformation, Yield and Fracture of Polymers, The Institute of Materials, London, pp. 64/1-64/4, 1994.

2. Wiegand, D., "Critical Strain for Failure of Highly Filled Polymer Composites", 3rd International Conference on Deformation and Fracture of Composites, University of Surrey Guildford, UK, pp. 558-567, 1995.

3. Wiegand, D. A., "Constant Critical Strain for Mechanical Failure of Several Particulate Polymer Composites and Other Materials", 20th Army Science Conference 1996, Proceedings, Vol I pp. 63-68, and Picatinny Arsenal Technical Report ARAED-TR-96020, July 1997.

4. Wiegand, D. A., "Mechanical Failure Properties of Composite Plastic Bonded Explosives", Proceedings of the American Physical Society Topical Conference in Shock Compression of Condensed Matter, eds. Schmidt, S. C., Dandekar, D. P., and Forbes, J. W., p 599, 1997.

5. Wiegand, D., Pinto, J., and Nicolaides, S., "The Mechanical Response of TNT and a Composite, Composition B, of TNT and RDX to Compressive Stress: I Uniaxial Stress and Fracture", J. Energetic Materials, 9, pp. 19-80, 1991; Wiegand, D. and Pinto, J., "Fracture of Composition B and TNT", Picatinny Arsenal Technical Report ARAED-TR-90038, April 1991, and Pinto, J., Nicolaides, S. and Wiegand, D., "Dynamic and Quasi Static Mechanical Properties of Comp B and TNT", Picatinny Arsenal Technical Report ARAED-TR-85004, November 1985.

6. Wiegand, D., "Bond Strength of Pressed Composites", Materials Research Society Symposium Proceedings, Interface Control of Electrical, and Mechanical Properties, eds. Murarka, S.P., Rose, K., Ohmim, T., and Seidel, T., Vol 318 pp. 387-392, 1994, and "Influence of Added Graphite on the Mechanical Strength of Pressed Plastic Bonded Explosives", Picatinny Arsenal Technical Report ARAED-TR-95018, January 1996.

7. Wiegand, D. A., "Damage Relationships Due to Compression of Polymer Composites", Bull Am Phys Soc 41, No 1, p 676, 1996.

8. Wiegand, D. A., "Thermally Activated Processes Evident from the Stress versus Strain Behavior of Particulate Polymer Composites", Bull Am Phys Soc, 42, No. 1, p 97, 1997.

9. Wiegand, D. A., "Mechanical Properties and Mechanical Failure of Plastic Bonded Explosives and other Energetic Materials," Proceedings of the 11th International Detonation Symposium, Snowmas, CO, 30 Aug 98, in press.

10. Dienes, J. K., "Strain-Softening of a Brittle Material via SCRAM", Los Alamos National Laboratory Report, in preparation.

11. Dienes, J. K. and Riley, N., "Strain-Softening of PBX-9501", Los Alamos National Laboratory Report, in preparation.

12. Trevino, S. F., and Wiegand, D. A., "SANS and SAXS Microstructure Study of Fractured Composites", Materials Research Society Meeting December 1996 and Proceedings of the 21st Army Science Conference, 15 Jun 98, Norfolk, VA, to be published.

13. Idar, D. J., Peterson, P. D., Fugard, C. S. and Gray, G. T., "Low Strain Rate Mechanical Properties of HE", Twentieth Semiannual Meeting of TCG1, Lawrence Livermore National Laboratory, 2-3 December 1997.

14. Idar, D., J., Peterson, P. D., Scott, P. D. and Funk, D. J., "Low Strain Rate Compression of PBXN-9, PBX 9501 and Mock 9501", LA-UR-97-2641 and Proceedings of the American Physical Society Topical Conference in Shock Compression of Condensed Matter, eds. Schmidt, S. C., Dandekar, D. P., and Forbes, J. W., p 582, 1997.

15. Aidun, J., Personal Communication.

16. Gazonas, G. A., "A Uniaxial Nonlinear Viscoelastic Constitutive Model With Damage for M30 Gun Propellant", Technical Report ARL-TR-115, 1993.

17. Gazonas, G. A., "A Uniaxial Nonlinear Thermoviscoelastic Constitutive Model With Damage for M30 Gun Propellant", Technical Report ARL-TR-469, 1994.

18. Seely, F. B., and Smith, J. O., Advanced Mechanics of Materials, New York, John Wiley and Sons, pp. 76-91, 1952.

19. Ewalds, H. L. and Wanhill, R. J. H., Fracture Mechanics, Baltimore, MD, Edward Arnold, pp. 6-19, 1984.

20. Dobratz, B. M. and Crawford, P. C., "LLNL Explosives Handbook, Properties of Chemical Explosives and Explosive Simulants", Lawrence Livermore National Laboratory Report UCRL-52997 Change 2, p 6-6 and p 6-8, 1985.

21. Flowers, G. L., Personal Communication.

22. Baudler, B., Hutcheson, R., Gallant, M. and Leahy, J., "Characterization of PBSW-9", NSWC TR 86-334, August 1989.

DISTRIBUTION LIST

Commander
Armament Research, Development and Engineering Center
U.S. Army Tank-automotive and Armaments Command
ATTN: AMSTA-AR-WEL-T (2)
AMSTA-AR-GCL
AMSTA-AR-WEE-D, B. Fishburn
M. Mezger
Y. Lanzerotti
D. Wiegand (15)
C. Hu
S. Nicolich
R. Surapaneni
AMSTA-AR-WEE-C, E. Baker
J. Orosz
AMSTA-AR-AES
AMSTA-AR-WEE, D. Downs
AMSTA-AR-QAR-R, L. Monole
E. Bixon
AMSTA-AR-QAR-V, F. Hildebrant
AMSTA-AR-WEE-B, M. Paduano
AMSTA-AR-WEA, R. Rupel
S. Cytron
AMSTA-AR-WES, A. E. Siklosi
D. Fair
Picatinny Arsenal, NJ 07806-5000

Defense Technical Information Center (DTIC)
ATTN: Accessions Division (12)
8725 John J. Kingman Road, Ste 0944
Fort Belvoir, VA 22060-6218

Director
U.S. Army Materiel Systems Analysis Activity
ATTN: AMXSY-EI
392 Hopkins Road
Aberdeen Proving Ground, MD 21005-5071

Commander
Chemical/Biological Defense Agency
U.S. Army Armament, Munitions and Chemical Command
ATTN: AMSCB-CII, Library
Aberdeen Proving Ground, MD 21010-5423

Director
U.S. Army Edgewood Research, Development and Engineering Center
ATTN: SCBRD-RTB (Aerodynamics Technology Team)
Aberdeen Proving Ground, MD 21010-5423

Director
U.S. Army Materiel Sytems Analysis Activity
ATTN: AMXSY-D
Aberdeen Proving Ground, MD 21005-5006

Director
U.S. Army Research Laboratory
ATTN: AMSRL-OP-CI-B, Technical Library
AMXBR-BLT, R. Frey
AMXBR-BLC, J. Starkenberg
P. Baker
AMXBR-TBT, R. Lieb
G. Gazonas
Aberdeen Proving Ground, MD 21005-5066

Chief
Benet Weapons Laboratory, CCAC
Armament Research, Development and Engineering Center
U.S. Army Tank-automotive and Armaments Command
ATTN: AMSTA-AR-CCB-TL
AMSTA-AR-LCB-RA, J. Vasilakis
Watervliet, NY 12189-5000

Director
U.S. Army TRADOC Analysis Command-WSMR
ATTN: ATRC-WSS-R
White Sands Missile Range, NM 88002

Commander
Naval Air Warfare Center Weapons Division
1 Administration Circle
ATTN: Code 473C1D, Carolyn Dettling (2)
China Lake, CA 93555-6001

GIDEP Operations Center
P.O. Box 8000
Corona, CA 91718-8000

Office of the Secretary of Defense
OUSDA(A)
Director, Live Fire Testing
Washington, DC 20301-3110

Director
U.S. Army Aviation Research and Technology Activity
Ames Research Center
Moffett Field, CA 94035-1099

Commander
U.S. Army Missile Command
ATTN: AMSMI-RD-CS-R (DOC)
Redstone Arsenal, AL 35898-5010

HQDA (SARD-TR)
Washington, DC 20310-0001

Commander
U.S. Army Materiel Command
ATTN: AMCDRA-ST
5001 Eisenhower Avenue
Alexandria, VA 22333-0001

Commander
U.S. Army Laboratory Command
ATTN: AMSLC-DL
Adelphi, MD 20873-1145

Commandant
U.S. Army Infantry School
ATTN: ATSH-CD-CSO-OR
Fort Benning, GA 31905-5660

Commander
U.S. Army Aviation Systems Command
ATTN; AMSAV-DACL
4300 Goodfellow Blvd
St. Louis, MO 63120-1798

Commander
U.S. Army Research Office
ATTN: Chemistry Division
P.O. Box 12211
Research Triangle Park, NC 27709-2211

Commander
Naval Weapons Center
ATTN: L. Smith
A. Amster
R. Reed, Jr.
China Lake, CA 93555

Commander
Ballistic Missile Defense Advanced Technology Center
ATTN: D. Sayles
P.O. Box 1500
Huntsville, AL 35807

Air Force Armament Technology Laboratory
ATTN: AFATL/DOIL
AFATL/DLODL
Eglin Air Force Base, FL 32542-5438

Southwest Research Institute
ATTN: M. Cowperthwaite
6220 Culebra Road
Postal Drawer 28510
San Antonio, TX 78284

New Mexico Institute of Mining and Technology
ATTN: TERA, T. Joyner
Campus Station
Socorro, NM 87801

Director
Lawrence Livermore National Laboratory
ATTN: R. McGuire
K. Scribner
M. S. Costantino
J. Forbes
L-324
M. Finger
P.O. Box 808
Livermore, CA 94550

Director
Los Alamos National Laboratory
ATTN: J960, J. Ramsay
MS B214, J. Dienes
MS P952, J. Dick
MS J567 D. J. Funk
MS C920, D. Idar
B. Asay
R. Gray
P.O. Box 1663
Los Alamos, NM 87115

Southwest Research Institute
ATTN: H. J. Gryting
P.O. Box Drawer 28510
San Antonio, TX 78284

Honeywell, Inc.
ATTN: R. Tompkins
10400 Yellow Circle Drive
MN 38-330
Minnetonka, MN 55343

Commander
U.S. Army Armament Munition and Chemical Command
ATTN: AMSMC-ESM, W. D. Fortune
AMSMC-IRD, G. H. Cowan
Rock Island, IL 61299-6000

Director
Sandia National Laboratory
ATTN: MS 432, J. Aidun
MS 437, R. Thomas
MS 477, T. Chen
Box 5800
Albuqure, NM

Johns Hopkins University
Applied Physics Laboratory
Chemical Propulsion Information Agency
ATTN: John Hannum
Johns Hopkins Road
Laurel, MD 20707

Morton Thiokol, Inc.
Louisiana Division
ATTN: Lee C. Estabrook
P.O. Box 30058
Shreveport, LA 71130

Commander
Naval Weapons Station
ATTN: L. Rothstein
Code 50 – NEDED
Yorkstown, VA 23491